Applied Catalysis B: Environmental 95 (2010) 110–119

Contents lists available at ScienceDirect

Applied Catalysis B: Environmental

journal homepage: www.elsevier.com/locate/apcatb

$FeAl_{12}$-Keggin type cation as an active site source for Fe,Al-silica mesoporous catalysts

M.N. Timofeeva *, M.E. Malyshev, V.N. Panchenko, A.N. Shmakov, A.G. Potapov, M.S. Mel'gunov

Boreskov Institute of Catalysis SB RAS, Prospekt Akad. Lavrentieva 5, 630090 Novosibirsk, Russian Federation

ARTICLE INFO

Article history:
Received 28 September 2009
Received in revised form 10 December 2009
Accepted 17 December 2009
Available online 23 December 2009

Keywords:
Fe,Al-containing mesoporous mesophase materials
Fe,Al-pillared clay
Hydrogen peroxide
Phenol
Oxidation

ABSTRACT

Iron-containing mesoporous mesophase materials Fe,Al-MMM-2 have been synthesized according to a sol-mesophase route under mild acidic conditions (pH 2.3–4.4) using Keggin type cation $[FeAl_{12}O_4(OH)_{24}(H_2O)_{12}]^{7+}$ ($FeAl_{12}^{7+}$) as Al and Fe sources. Effect of pH of the synthetic solution on structural and physicochemical properties of Fe,Al-MMM-2 has been evaluated by means of small- and wide-angle XRD, FTIR, DR-UV–vis, and N_2-adsorption/desorption analysis. It has been established that deviation of stability of $FeAl_{12}^{7+}$ cation at various pH determines Al/Fe ratio in the resulting material as 12/1 (material synthesized at pH 4.4), and 6/1 (pH 2.4 and 3.3). Correlation between incorporation of Al and Fe in different forms and resulting materials texture is discussed. Fe,Al-MMM-2 materials have been tested as catalysts for wet phenol oxidation with H_2O_2. Insertion of Al species into the framework of the silicate matrix increases the activity comparing to a reference Fe,Al-pillared clay due to both higher surface acidity and lower diffusion limitations that correspond to Fe,Al-MMM-2.

1. Introduction

Nowadays, one of the routes to destroy phenol, which is known to be toxic, is its complete destruction to harmless compounds, e.g. CO_2 and water. Both homogeneous systems of the Fenton-type (Fe^{3+}/Fe^{2+}–H_2O_2) and heterogeneous Fenton-type systems are viewed as perspective catalysts for this aim. Fe-containing microporous materials such as Fe-ZSM-5 [1] and Fe-pillared clays [2,3] have attracted considerable attention due to their ability of the effective phenol oxidation. Unfortunately, catalytic activity of these materials depends on diffusion limitation in liquid-phase reactions. Moreover, their activity in phenol oxidation with H_2O_2 is maximal at pH 3–4 that favours substantial iron leaching.

Iron-containing mesoporous mesophase materials (Fe-MMMs) are of particular interest due to their unique textural, physicochemical and catalytic properties. Because of the pore sizes in a range of several nanometres, their internal surface is opened for a much wider assortment of reagents comparing to microporous systems [4]. Fe-MMMs can be used in various catalytic reactions, but the most common choices are the Fenton-type processes [5,6]. Fe-MMMs were demonstrated to be useful in phenol destruction in aqueous media despite on strong dependence of Fe-MMMs activity on pH of the reaction mixture [7–9]. The maximum catalytic activity of Fe-MMMs is observed at pH 3.0–3.7 of phenol aqueous solution, where iron leaching is substantial. It was demonstrated earlier that after 15 min from the beginning of the reaction 100% phenol conversion is achieved over fresh Fe-MCM-41 and Fe-HMS type catalysts. However, these materials suffer from destruction of the mesopores, iron agglomeration and leaching (the latter comprises from 6 to 100 wt.% from initial value) [7].

According to Xianga et al. [10] a basis of method of iron insertion in SBA-15 effects the iron state in sample. Thus, iron oxide isolated species (~7–8 nm) can be obtained by classical wet impregnation procedure. Iron oxide species of smaller size (~2–4 nm) homogeneously dispersed within structure of the SBA-15 can be produced via self-combustion of an impregnated iron–glycinic complex. The catalytic activity of the resulting ferrosilicates, as well as their stability, is strongly related to the dispersion of the active phase, and accessibility of Fe^{3+} for reagent adsorption. Impregnated Fe-SBA-15 samples manifest high activity, however, substantial iron leaching is usually observed in aqueous media. In contrast, materials that contain relatively large iron oxide clusters embedded in the silica matrix and dispersed iron species incorporated in the silica walls of Fe-SBA-15 prepared due to the co-precipitation of silica and iron sources are proved to be more efficient Fenton-type catalysts [10].

Variation of coordination environment of iron atoms in mesoporous silicates allows adjusting both catalytic properties and resistance to iron leaching [5,6]. According to Kawabata et al. [7] iron leaching was negligible when Fe^{3+} was incorporated into

* Corresponding author. Tel.: +7 383 330 72 84; fax: +7 383 330 80 56.
E-mail address: timofeeva@catalysis.ru (M.N. Timofeeva).

0926-3373/$ – see front matter © 2009 Elsevier B.V. All rights reserved.
doi:10.1016/j.apcatb.2009.12.016

the framework of MCM-41, whereas small iron oxide clusters leached out during the liquid-phase reactions. In our previous work [11] we also demonstrated that site-isolated iron species located in Fe-containing mesoporous materials (Fe-MMM-2) synthesized under mild acidic conditions (pH 1–2.4) are stable to leaching and structure deformation. In addition Fe-MMM-2 was found to be highly active in phenol oxidation with H_2O_2. Moreover we have found that pH of the synthetic mixture during Fe-MMM-2 preparation allows adjusting iron state and thus influences catalytic activity. Isolated iron species predominate in silica framework below Fe content of ~1 wt.% and pH of synthetic mixture below 2.0, or Fe content lower than 2 wt.% and pH ~1.0. The highest specific catalytic activity was observed for the Fe-MMM-2 catalyst synthesized at pH 1.0 and Fe ~1.7 wt.%. Unfortunately, this sample was less active than the known most active system, namely Fe,Al-pillared clay which was prepared by exchanging of the charge-compensating cations in the interlamellar space of the montmorillonite clay with mixed Fe,Al-polyoxocations of Keggin structure $[FeAl_{12}O_4(OH)_{24}(H_2O)_{12}]^{7+}$ ($FeAl_{12}^{7+}$) [12]. The lower activity of Fe-MMM-2 comparing to Fe,Al-PILC is very likely related to the differences in strength and amount of acidic surface sites.

One can consider insertion of Al-ions in Fe-containing mesoporous materials as a way to increase in the surface acidity of Fe-MMMs. Unfortunately, the information on mesoporous Fe,Al-silicates is very insufficient so far. According to Vinu et al. [13] the simultaneous incorporation of trivalent atoms (Fe and Al) into the walls of MCM-41 and variation of $n_{Si}/(n_{Fe} + n_{Al})$ ratio permit the adjustment of the strength and amount of acid sites. A highly active heterogeneous Fenton catalyst was synthesized by impregnating iron oxide nanoparticles into alumina coated mesoporous SBA-15 silica [14]. It was shown that the increase of Al content enforces the dispersion of iron oxide nanoparticles, and the subsequent increase of the rate of dye RB5 degradation and decrease of the rate of H_2O_2 degradation. The increase of catalytic activity due to the increase in surface acidity was observed in phenol oxidation over Fe,Al-MCM-41 [15] synthesized by wet impregnation of Al-MCM-41 with $Fe(NO_3)_3$.

In general, the known syntheses of Fe,Al-containing mesoporous systems were provided at pH 10–11.5 [14,15]. But this is very narrow range, and it is well-known, that pH has strong effect on the properties of mixed Fe,Al-hydrolyzed solutions, because the structure of the species in the solutions is of particular importance for the synthesis of Fe- and Al-containing silicate systems. Effect of a type of mixed Fe,Al-hydrolyzed solution on textural, physicochemical and catalytic properties was extensively studied elsewhere for Fe,Al-pillared clays (Fe,Al-PILCs), which usually are prepared by ion exchange with mixed Fe,Al-polyoxocations [12] (for example, Keggin type polyoxocation $FeAl_{12}^{7+}$). After calcination the inserted polycations yield rigid, thermally stable oxide species, which prop up the clay layers and prevent their collapse. However, one should take into account the behaviour of Fe,Al-polyoxocations, which differs depending on pH of their aqueous solutions. The formation of this polyoxocation strongly depends on OH/(Al + Fe) and Al/Fe ratios. Thus, these synthetic parameters direct the adjustment of textural properties of Fe,Al-PILCs and the state of iron atoms [12,16]. The most preferable region of $FeAl_{12}^{7+}$ existence is OH/(Al + Fe) ratio is 2.0–2.4. Isolated iron species predominate when OH/(Fe + Al) ratio is 2.4 and Al/Fe is lower than 10/3. Noteworthy, Fe,Al-PILCs allow carrying out hydroperoxide organic pollutants oxidation at pH 6.0–6.2 due to their high surface acidity [12]. However, as Fenton-type systems their activity in phenol oxidation with H_2O_2 is maximal at pH 2.5–4.0 and is accompanied with substantial iron leaching.

In this work, we report the synthesis of Fe,Al-containing mesoporous mesophase materials (Fe,Al-MMM-2) according to a previously reported sol-mesophase route under mild acidic conditions using Keggin type cation $FeAl_{12}^{7+}$ as Al and Fe sources. The effect of the synthesis pH and iron content on the textural properties and the iron state are discussed. The catalytic properties of Fe,Al-MMM-2 evaluated in oxidation of phenol with hydrogen peroxide are shown. The correlation between the preparation conditions, iron state, catalytic activity and stability to leaching are established. The catalytic performance of Fe,Al-MMM-2 is compared with the activities of iron-containing mesoporous Fe-silicates (Fe-MMM-2) reported earlier [11] and microporous Fe,Al-pillared clay (Fe,Al-PILC) [8].

2. Experimental

2.1. Materials

Fe,Al-PILC(4.4) was prepared from sodium containing layered aluminosilicate (Na-clay) following a procedure described in Ref. [12]. The Na-clay was synthesized by the treatment of the natural montmorillonite (Mukhortala bed located in Buryatia, Russian Federation) with 1 M NaCl at a ratio of 1/100 (w/w) between solid and liquid phases at 80 °C for 2 h. This clay was ground and sieved to obtain a fraction of 20–40 μm, dispersed in distilled water (1 wt.% mixture) and stirred for about 24 h at 20 °C followed by redispersion in an ultrasonic bath. The Al,Fe-pillaring solutions (Al/Fe = 10/1) were prepared by mixing of 0.2 M $AlCl_3$ and 0.1 M $FeCl_3$ with following hydrolysis using NaOH solution (OH/(Al + Fe) = 2.4 mol mol^{-1}). The obtained solution was added (0.6 ml/min) to the clay at room temperature and the mixture was stored for 21 days at room temperature. The intercalated clay was filtered, washed with distilled water, dried and calcined in air at 500 °C for 2 h.

The synthesis of Fe-containing materials (Fe,Al-MMM-2 and Fe-MMM-2) was performed using sol-mesophase route under mild acidic conditions. The advantage of this route is in the absence of traditional autoclave hydrothermal stage, while the obtained materials show excellent stability and activity in liquid-phase oxidation of hydrocarbons with hydrogen peroxide. Note that absence of hydrothermal treatment does not allow designation of this preparation route as "hydrothermal synthesis" known from the literature. The designation of the samples and the main conditions of this synthesis are given in Table 1. Si-MMM-2 was synthesized using aqueous $Na_2Si_2O_5$ as a silica source. The 0.2 M

Table 1
Specification of Fe-containing samples.

Designation of sample	Preparation gel		Fe-containing product				
	pH[a]	Fe/Si (mol mol^{-1})	Fe (wt.%)	Al (wt.%)	Na (wt.%)	Al/Fe (mol mol^{-1})	Fe/Si (mol mol^{-1})
Si-MMM-2(2.4)	2.4	–	–	–	0.01	–	–
Fe-MMM-2(2.4)	2.4	0.020	1.7 ± 0.1	0	0.01	–	0.020
Fe,Al-MMM-2(2.4)	2.4	0.020	1.1 ± 0.1	3.1 ± 0.1	0.07	6/1	0.0126
Fe,Al-MMM-2(3.3)	3.3	0.020	1.0 ± 0.1	3.0 ± 0.1	0.01	6/1	0.0126
Fe,Al-MMM-2(4.4)	4.4	0.020	1.1 ± 0.1	6.4 ± 0.1	0.04	12/1	0.0130
Fe,Al-PILC(4.4)	2.4	–	1.7 ± 0.1	13.8 ± 0.1	–	–	–

[a] pH of medium during synthesis.

aqueous solution of cetyltrimethylammonium bromide (CTAB) (pH 1.0, HCl) and 0.12 M aqueous solution of a silica sol (pH 1.0, HCl) were mixed in Si/CTAB ~5 mol mol^{-1} and pH was adjusted to pH ~2.4 by a slow addition of an aqueous solution of NaOH (conc.). After mixing the synthetic mixture was kept at 323 K for 24 h. The resulting precipitate was filtered off, washed with distilled water, dried in air at room temperature for 24 h, and calcined at 773 K for 8 h. Fe-MMM-2(2.4) was synthesized by analogy at pH 2.4 [11] using aqueous $Na_2Si_2O_5$ and $FeCl_3\ 6H_2O$ as silica and Fe sources, respectively. Fe content in this sample was 1.7 wt.%.

Fe,Al-MMM-2 samples were prepared in a similar manner at various pH of synthetic mixture. Generally, materials' preparation included mixing of three solutions: (1) 0.2 M aqueous solution of cetyltrimethylammonium bromide (CTAB) (pH 1.0, HCl), (2) 0.12 M aqueous solution of a silica sol (pH 1.0, HCl) and (3) aqueous solution of $[FeAl_{12}O_4(OH)_{24}(H_2O)_{12}]^{7+}$ (Fe 2 g L^{-1}, pH 4.4 [17]). The solutions were mixed in the required proportions, and pH was adjusted to 2.4, 3.3 and 4.4 by a dropwise addition of an aqueous solution of NaOH (conc.). The molar ratio of Si/CTAB was chosen to be 5.0. In turn, the amount of $FeAl_{12}^{7+}$ solution was calculated to achieve the iron content in the resulting catalysts of about 1.7 wt.% for more appropriate comparison with a previously synthesized Fe-MMM-2 catalyst. After mixing the synthetic mixture was kept at 323 K for 24 h. The resulting precipitate was filtered off, washed with distilled water, dried in air at room temperature for 24 h, and calcined at 773 K for 8 h.

2.2. Catalyst characterization

Textural characteristics of Fe-containing samples were determined from nitrogen adsorption isotherms (77 K, Autosorb-6B (Quantachrome)). Software supplied with instrument includes procedure of pore volume-size calculations based on NLDFT method with kernel functions for silica and cylinder geometry. This procedure was applied to calculate pore volume-size distributions in this work.

The X-ray diffraction patterns were measured on an X-ray diffractometer XTRA (ThermoARL) with Cu-K_α (λ = 1.5418 Å) radiation. The DR-UV–vis spectra were recorded on a UV-2501 PC Shimadzu spectrophotometer with a IRS-250A accessory in the 190–900 nm range with a resolution of 2 nm. $BaSO_4$ was used as a standard.

For IR transmission measurements, the samples were pressed into self-supporting wafers (density of the obtained wafers was measured and had values in a range of 7–20 mg cm^{-2}) and pretreated within the IR cell by heating at 450 °C under air flow for 1 h and under vacuum for 1 h at 300 °C before adsorption experiments. CO adsorption was carried out at 80 K under equilibrium pressures of P_{CO} from 0.5 to 76 torr. For spectral studies Fe-containing samples were exposed to saturated $CDCl_3$ vapour for 3 min at room temperature. IR spectra of adsorbed $CDCl_3$ are presented as difference spectra of the sample before and after $CDCl_3$ adsorption. FTIR spectra were recorded on a Shimadzu FTIR-8300 spectrometer in the range of 400–6000 cm^{-1} with a resolution of 4 cm^{-1}, accumulating 50 scans.

The iron content in the samples was determined by means of the following procedure. The iron was leached out into solution in the form of Fe^{3+} ions by reflux of Fe-containing sample in HCl (37 wt.% in water) at 100 °C and then the solution was titrated with 1,10-phenanthroline. After an appropriate calibration, the absorbance of the iron–phenanthroline complex measured by UV–vis at λ = 510 nm was recalculated to Fe content (test-sensitivity is 10^{-7} g ml^{-1}). The Na content in samples was determined by atomic absorptive analysis (AAS Solaar M 6 spectrometer). The Al content in samples was determined by UV–vis method. The Al-containing sample was fused with $Na_2B_4O_7$–Na_2CO_3–KNO_3 mixture and then it was dissolved in HCl (HCl:H_2O 1:3, v/v). The aurintricarboxylic acid was added to the obtained solution and the absorbance of the aluminium–aurintricarboxylic acid complex was measured at λ = 520 nm.

2.3. Catalytic tests

The wet full phenol oxidation was carried out at 40–60 °C in a glass temperature-controlled vessel equipped with a magnetic stirrer and a reflux condenser. Mixture of phenol/H_2O_2 = 1:14 mol mol^{-1} (20 ml of 1 mM phenol solution in water) and a catalyst (1.0 g L^{-1}) was placed into the reactor. The phenol concentration in the solution was measured using appropriate UV–vis technique (Specord UV–VIS M-40 instrument, λ = 273 nm, accuracy of measurements ±10%). The concentration of H_2O_2 was determined by iodometric titration.

The phenol hydroxylation was carried out at 40 °C in the same vessel. Mixture of phenol/H_2O_2 = 1:2 mol mol^{-1} (10 ml of 0.1 M phenol solution in water) and a catalyst (1.0 g L^{-1}) was placed into the reactor. The identification and determination of the products (hydroquinone (QH) and catechol (CH)) were performed by using a Shimadzu Prominence HPLC system equipped with Pathfinder 100 AS 2.5 UM column.

H_2O_2 degradation over Fe-MMM-2 and Fe,Al-MMM-2 was studied in a glass thermostated reactor under stirring at 60 °C. The reactor was loaded with 20 mg of sample and 20 ml of H_2O_2 aqueous solution (0.16 M). Aliquots were taken after regular time intervals, and the concentration of H_2O_2 was determined by iodometric titration.

2.4. Phenol and ACDB adsorption measurements

Phenol adsorption over Fe-containing samples was studied in a glass thermostated reactor under stirring at 25 °C. The reactor was loaded with 50 mg of Fe-containing sample and 10 ml of a phenol aqueous solution (10 mM). Aliquots were taken after regular time intervals, and the phenol concentration was determined by analysis of corresponding UV–vis (λ = 273 nm) spectra.

The monoazo dye acid chrome dark-blue ($C_{16}H_9O_9Na_2ClS_2N_2$, ACDB) adsorption onto Fe-containing samples was studied in a glass thermostated reactor under stirring at 50 °C. The reactor was loaded with 50 mg Fe-containing sample and 5 ml of a ACDB aqueous solution (1×10^{-4} M). At regular time intervals, aliquots were taken and the ACDB concentration was determined by UV–vis at λ = 510 nm.

3. Results

3.1. Structure and texture of Fe,Al-MMM-2

To perform the design of Fe,Al-containing mesoporous molecular sieves using Keggin type cation $FeAl_{12}^{7+}$ as Al and Fe sources, we proceeded from basis of our present knowledge. Firstly, in our earlier publications we demonstrated that pH of the synthetic solution affects both the textural characteristics, state and leaching ability of iron atoms in Fe-MMM-2 [11]. The optimal pH range for the preparation of Fe-MMM-2 containing site-isolated iron species, which was stable to leaching and highly active in phenol oxidation with H_2O_2, was 1.0–2.0 at 1.0–2.0 wt.% iron content. Secondly, one should take into account that the pH region of 3.7–4.8 within which $FeAl_{12}^{7+}$ polyoxocation is stable [12,18]. The high acidity (pH <3.3) is beneficial to the decomposition of mixed $FeAl_{12}^{7+}$ cation. According to ^{27}Al NMR spectroscopic data $FeAl_{12}^{7+}$ polyoxocation is stable in reaction mixture of $FeAl_{12}^{7+}$/$Na_2Si_2O_5$/CTAB prepared at pH 4.4, because signal at 62.5 ppm attributed to Al atoms in fourfold coordination within a polymeric structure

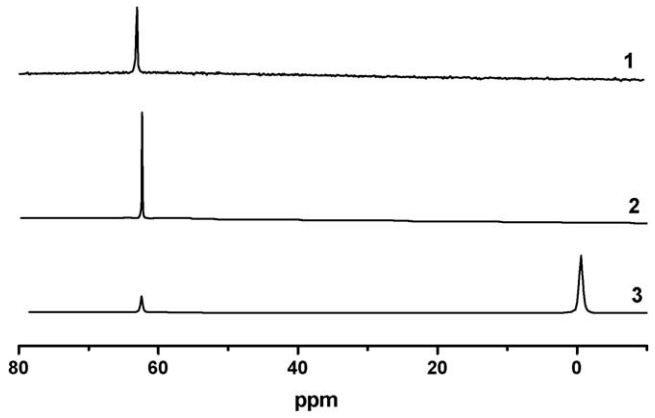

Fig. 1. ^{27}Al NMR spectra of aqueous Fe,Al-solution prepared at OH/(Fe + Al) = 2.4 and Al/Fe = 12/1 (1), reaction mixture of $Al_{12}Fe^{7+}/Na_2Si_2O_5$/CTAB prepared at pH 4.4 (2), and reaction mixture of $Al_{12}Fe^{7+}/Na_2Si_2O_5$/CTAB prepared at pH 3.3 (3).

Al_{13}^{7+} complex [19] is observed in spectrum (Fig. 1). Note that this spectrum is similar to the spectrum of $FeAl_{12}^{7+}$ in water at pH 4.4. The increase of acidity leads to collapse of $FeAl_{12}^{7+}$ polyoxocation and signal at 0 ppm assigned to monomeric Al species [20,21] reveals in spectrum of reaction mixture of $FeAl_{12}^{7+}/Na_2Si_2O_5$/CTAB prepared at pH 3.3 (Fig. 1, spectrum 3).

Therefore, a great care must be kept in the synthesis of Fe,Al-containing mesoporous materials using $FeAl_{12}^{7+}$ cations, in which properties would reveal optimum combination between catalytic activity and stability. Thus, we synthesized corresponding Fe,Al-containing mesoporous samples Fe,Al-MMM-2 at pH 2.4, 3.3 and 4.4 at 1.0–1.1 wt.% of iron content. Tables 1 and 2 summarize the results of the chemical analysis, textural characteristics and mesopore interlayer spacing (d_{10}) of the Fe,Al-MMM-2 samples. Table 2 suggests that pH of the synthetic solution influences on the texture characteristics of Fe,Al-MMM-2. Adsorption/desorption isotherms of N_2 at 77 K for Fe,Al-MMM-2, and corresponding pore volume-size distributions are shown in Fig. 2A. The shape of the isotherms and distributions is characteristic of mesoporous structures with uniform pores. All Fe,Al-MMM-2 samples have large surface areas of 1100–1600 $m^2\ g^{-1}$. The external surface area of mesoporous aggregates for these samples is substantially higher than that for Si-MMM-2 and Fe-MMM-2(2.4). One can see that the mesopore diameters for Fe,Al-MMM-2 samples are larger (3.3–3.7 nm) comparing to the Si-MMM-2 (3.3 nm) and Fe-MMM-2(2.4) (3.1 nm). Pore volume, surface area, and the mean pore diameter of Fe,Al-MMM-2(4.4) is lower than that of Fe,Al-MMM-2(2.4) and Fe,Al-MMM-2(3.3). Besides of these differences a slight broadening of the PVSD is observed for Fe,Al-MMM-2(4.4).

Fig. 2B shows low-angle XRD patterns for Si-MMM-2 and Fe,Al-MMM-2. The reflex at 2.4°, which likely corresponds to diffraction from 10 planes of the poorly ordered 2D hexagonal mesostructure was observed earlier in XRD patterns of Si-MMM-2 [22]. Addition of Fe,Al-complex into the synthetic solution results in a shift of 10 reflex from 2.4° to 2.19° for the samples synthesized at pH 2.4 and 3.3. This is accompanied with this reflex sharpening and appearing of a wide reflex at 3–4.5°. The latter is most probably a superposition of diffraction from 11 and 20 planes that are characteristic to 2D hexagonal structures. Increase of pH of synthetic mixture to 4.4 results in a backward shift of 10 reflex to wider angles and decreasing of the intensity of reflection in 3–4.5° region. The reflection in the 2θ region of 20–30° indicates the presence of amorphous silicate phase in Fe,Al-MMM-2 (Fig. 2B) [23,24].

The observed differences between pure siliceous Si-MMM-2, iron-containing silicate Fe-MMM-2, and Fe,Al-MMM-2 suggest that presence and state of Fe-containing polyoxocation definitely affect material structure and texture. As one can see from the data shown in Table 2, the wall thickness of Fe-MMM-2 synthesized at pH 2.4 is slightly higher (1.3 nm) comparing to the pure siliceous Si-MMM-2 (1.0 nm). This can be explained by the incorporation of larger ions Fe^{3+} (0.0645 nm) into the silica framework to replace smaller ions Si^{4+} (0.040 nm). At the same time the incorporation of larger mixed Fe,Al-ions into silica framework is possible if one assumes that pre-hydrolyzed silicate oligomeres mixed with Fe,Al-ions might react during the progress of the Fe,Al-MMM-2 formation [25,26]:

$$\{[Al_{13}O_4(OH)_{23}(H_2O)_{12}]^{7+}{-}OH\} + HO{-}[Si(OH)_2]_n{-}OH \rightarrow \{[Al_{13}O_4(OH)_{23}(H_2O)_{12}]^{7+}{-}O{-}[Si(OH)_2]_n{-}OH\} + H_2O$$

If so, by the analogy with Fe-MMM-2 the wall thickness in Fe,Al-MMM-2 should increase. And this is the case of the sample, synthesized at pH 4.4. The surface area of this material is slightly higher comparing to Si-MMM-2.

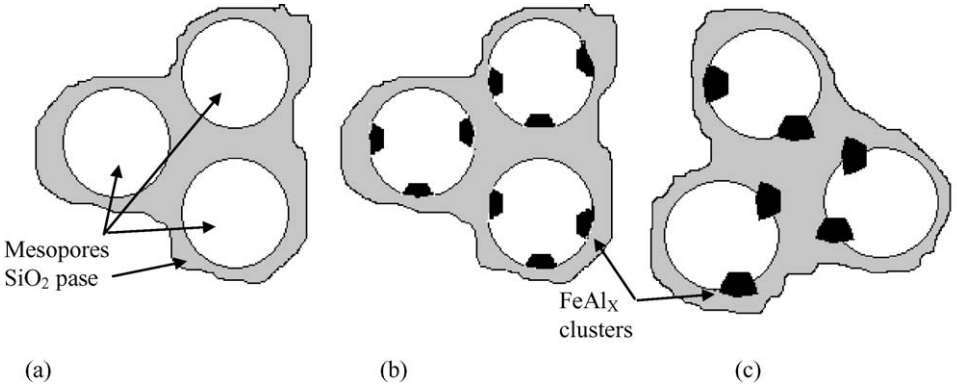

The wall thickness of Fe,Al-MMM-2 samples synthesized at pH 2.4 and 3.3 is lower than 1 nm and close to Si-MMM-2 material. Their surface areas are considerably higher comparing to Si-MMM-2. These data allow us to believe that at pH 4.4, when $FeAl_{12}^{7+}$ cations are stable they incorporate into silicate walls near to surface, making it more rough comparing to pure silicate. The latter is the reason of the surface area increase. The ease of silica sol coagulation in the presence of $FeAl_{12}^{7+}$ also may be one of the main reasons of incorporation of $FeAl_{12}^{7+}$ into silicate walls. It is well-known [27] that the coagulation process of various organic

Table 2
Structural and textural characteristics of Fe-containing samples.

Sample	A[a] ($m^2 g^{-1}$)	A_{ext}[b] ($m^2 g^{-1}$)	V_{meso}[c] ($cm^3 g^{-1}$)	D[d] (nm)	d_{10}[e] (nm)	a[f] (nm)	w[g] (nm)
Si-MMM-2	1195	10	0.61	3.3	3.7	4.3	1.0
Fe-MMM-2(2.4)	930	31	0.43	3.1	3.8	4.4	1.3
Fe,Al-MMM-2(2.4)	1518	149	0.90	3.7	3.9	4.5	0.8
Fe,Al-MMM-2(3.3)	1616	173	0.94	3.8	4.0	4.6	0.8
Fe,Al-MMM-2(4.4)	1315	177	0.56	3.3	3.8	4.4	1.2
Fe,Al-PILC(4.4)	215	109[h]	–	–	1.8	1.8	–

[a] A—specific surface area.
[b] A_{ext}—external surface area of mesopore aggregates.
[c] V_{meso}—mesopore volume.
[d] D—mesopore diameter.
[e] d_{10}—mesopore interlayer spacing ($a = (2/\sqrt{3})d_{10}$).
[f] a—unit cell parameter.
[g] w —pore wall thickness ($w = a - D$).
[h] Micropore surface area (A_{micro}) is 106 $m^2 g^{-1}$.

and inorganic substances in water at the presence Al and Fe hydroxides depends on pH (typically, optimum pH 4–6), and as a rule, pre-hydrolyzed mixture of Al and Fe is often more effective than simple Al and Fe salts. Due to this reason at pH <3.3 $FeAl_X$ clusters deposit on the surface not penetrating the walls, and thus not affecting walls structure. Simultaneously, $FeAl_X$ clusters introduce more roughness to the surface more pronouncedly increasing its area. Chemical analysis of Fe,Al-MMM-2 supports this assertion (Table 1). The same effect of the pH of the synthetic mixture influence on the textural parameters was observed for Fe-containing mesoporous materials elsewhere [28,29]. According to our recent data the wall thickness, interlayer distance and mesopore diameter slightly decreased when pH of the synthetic mixture increases from 0.5 to 2.4 [11].

3.2. Effect of pH on the iron state

The effect pH of the synthetic mixtures during the catalyst preparation on iron state was demonstrated earlier for Fe-SBA-15 [30] and Fe-MMM-2 [11]. According to DRS-UV–vis spectroscopy the iron cations in the silica matrix of Fe-MMM-2 have mainly tetrahedral coordination when Fe content is lower than 2 wt.% and synthetic pH is 1.0–2.0. The increase of iron content and/or synthetic pH favours the formation of iron oxide phase. As can be seen from Fig. 3 (line 4) two bands at 222 and 252 nm were observed in Fe-MMM-2(2.4) sample. This spectrum is similar to the spectra reported for microporous ferrisilicates [31,32], Fe-MCM-41 [7] and Fe-MCM-48 [33,34]. These bands are usually assigned to a low-energy charge transfer between the oxygen ligands and Fe^{3+} ions, i.e. the $t_1 \rightarrow t_2$ and $t_1 \rightarrow e$ transitions for Fe^{3+} in the [FeO_4] tetrahedral group. Unfortunately, these bands in the 200–300 nm region overlap with bands attributed to octahedral complexes of Fe^{3+} [35]. That is why these bands cannot be unambiguously ascribed to tetrahedral coordination state of Fe^{3+}. Interestingly, the shift of bands (222 → 209 nm and from 252 → 270 nm) is observed in spectrum of Fe,Al-MMM-2(2.4) (Fig. 3, line 1). Moreover, the increase in pH of the synthetic solutions leads to the decrease in the intensity of the band at 209 nm that clearly demonstrates some transformation in coordination of iron species in the samples. A weaker and broad band centred at ~370 nm can point out the formation of aggregated iron oxide clusters in Fe,Al-MMM-2 samples.

3.3. Surface acidity of Fe,Al-MMM-2

3.3.1. FTIR study of the surface OH-groups

The state of surface sites and their properties are most efficiently analyzed by IR spectroscopy. Fig. 4 shows FTIR spectra of Fe-MMM-2(2.4), Fe,Al-MMM-2(2.4), Fe,Al-MMM-2(4.4), and Fe,Al-PILC in the OH-stretching region. The narrow bands at 3745 and 3720 cm^{-1} and the broad bands in the range of 3650–3400 cm^{-1} are observed in IR spectra of all samples pre-heated at 450 °C in air and then at 300 °C in vacuum. The bands at 3745 and 3720 cm^{-1} are usually attributed to the stretching vibration of both isolated Si–OH groups and the isolated OH-groups from Si–OH and Al–OH which slightly interact with walls of aluminosilicates [36,37]. The intensity of these bands depends on the chemical composition of samples and pH of the synthetic mixture. Thus, intensities of these bands for Fe,Al-MMM-2(2.4) are nearly twice as much as that for Fe,Al-MMM-2(4.4). Weaker broad bands in the range of 3650–3400 cm^{-1} point to the presence of hydrogen

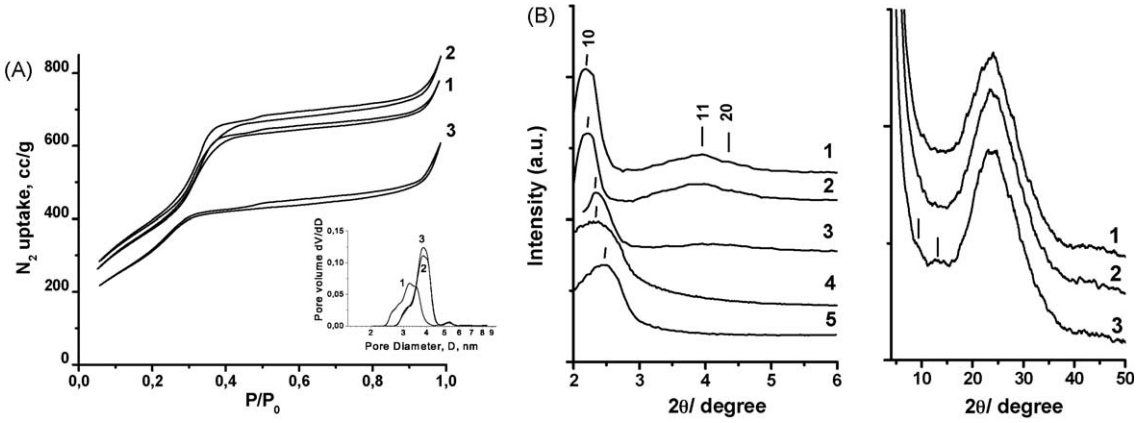

Fig. 2. (A) N_2 adsorption isotherms for Fe,Al-MMM-2 synthesized at various pH of medium during synthesis. Insert shows the corresponding pore volume-size distributions; (B) XRD patterns for Fe,Al-MMM-2 synthesized at pH 2.4 (1), pH 3.3 (2), pH 4.4 (3), Fe-MMM-2 synthesized at pH 2.4 (4) and Si-MMM-2 synthesized at pH 2.4 (5).

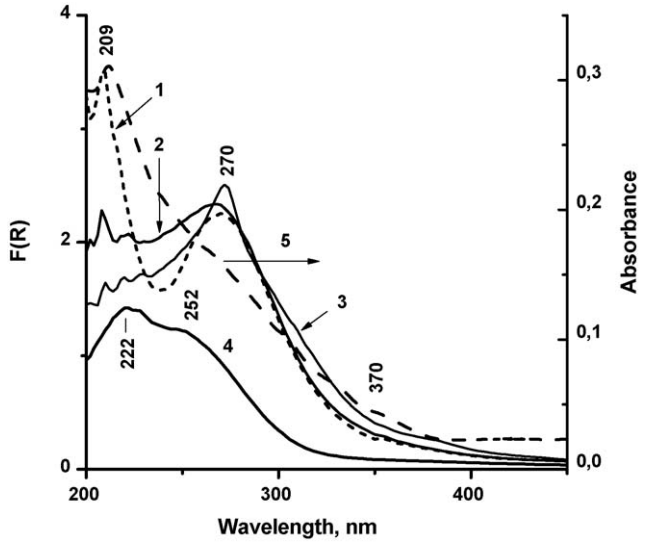

Fig. 3. DR-UV–vis spectra of Fe,Al-MMM-2 synthesized at pH 2.4 (1), pH 3.3 (2), pH 4.4 (3), Fe-MMM-2 synthesized at pH 2.4 (4), and UV–vis spectrum of Fe,Al-solution (5) ($AlCl_3$ 0.016 M, Al/Fe = 10/1, OH/(Fe + Al) = 2.4 (pH 4.4)) at 25 °C.

bonded OH-groups and strong Bronsted acid Al(OH)Si sites. A band at 3660 cm^{-1} is assigned to the structural Si(OH)Fe groups [37]. A similar band has been observed for ferrisilicates with MFI and β structures [38,39] and Fe-alumosilicate mordenite [37]. The comparison between spectra of Fe,Al-containing samples and spectrum of Fe-MMM-2(2.4) shows that the insertion of aluminium ions favours the increase in amount of hydrogen bonded OH-groups and strong Bronsted acid Al(OH)Si sites. However, the amount of these groups is higher in Fe,Al-PILC(4.4) comparing to Fe,Al-MMM-2 samples.

3.3.2. FTIR study of the surface OH-groups by low-temperature CO adsorption

The acid strength of solids can be estimated by FTIR spectroscopy using CO as probe molecule. CO is a weakly basic probe molecule which can adsorb through the carbon atom on OH-groups of our samples. Due to this interaction the vibrational frequencies of ν_{OH} and $\nu_{C\equiv O}$ modes will be shifted, which is proportional to the OH–CO interaction strength.

Fig. 5 shows the difference in the spectra of Fe-containing samples in the OH-stretching region after and before CO adsorption as a probe molecule at 80 K. One can see the band at 3745 cm^{-1} is converted into several broader bands at 3650–3655, 3610–3615, 3535–3548 and 3480 cm^{-1} after CO adsorption. These results clearly point to the presence of several types of $OH_{Bronsted}$ sites. The weaker band at 3650–3655 cm^{-1} and strong band at 3610 cm^{-1} are observed in IR spectra of Fe-MMM-2 and Fe,Al-MM-2(2.4) samples. The nearby position of bands in spectra can point to the proximity of acidity for these samples. At the same time the broad band at 3535 cm^{-1} appears in spectrum of Fe,Al-MMM-2(4.4), that indicate the formation of strong $OH_{Bronsted}$ sites. Note that bands at 3610–3615, 3535–3548 and 3480 cm^{-1} are assigned to bridging Si(OH)Al groups [40–42]. Unfortunately, the band of Si(OH)Fe group overlaps with bands attributed to bridging Si(OH)Al groups, that presents a real challenge for characterization of Fe and Al state in Fe,Al-containing samples. It should be remarked that low-frequency band at 3480 cm^{-1} observed in spectrum of Fe,Al-PILC suggests that these sample possesses more stronger acid sites than Fe-MMM-2 and Fe,Al-MMM-2 samples.

3.3.3. FTIR study of the strength of surface OH-groups by $CDCl_3$ adsorption

The strength of basic sites of samples can be estimated from data of $CDCl_3$ adsorption [43–45]. Fig. 6 shows the spectra of $CDCl_3$ adsorbed on Si-MMM-2 and Fe-containing samples. The main positions of the bands in their spectra are given in Table 3. One can see the absorption band at 2265 cm^{-1} in spectrum of $CDCl_3$ adsorbed on Si-MMM-2. It is slightly different from the band in the spectrum of gaseous $CDCl_3$ (ν_{CDCl_3} 2268 cm^{-1}). The bands at 2260 and 2265 cm^{-1} are observed in the spectrum of Fe-MMM-2 upon $CDCl_3$ dosage. Interestingly, after deconvolution three bands disclose in the spectra of Fe,Al-MMM-2(4.4) and Fe,Al-PILC samples (Fig. 6, spectra 3 and 4). According to Knozinger and

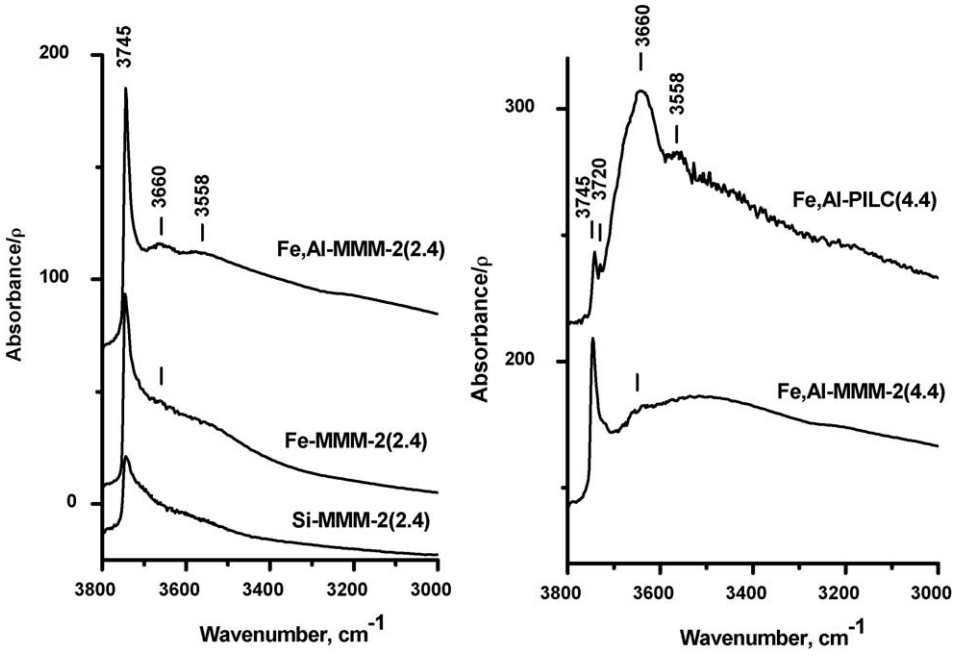

Fig. 4. FTIR spectra Fe-containing samples in the O–H stretching region before interaction with CO.

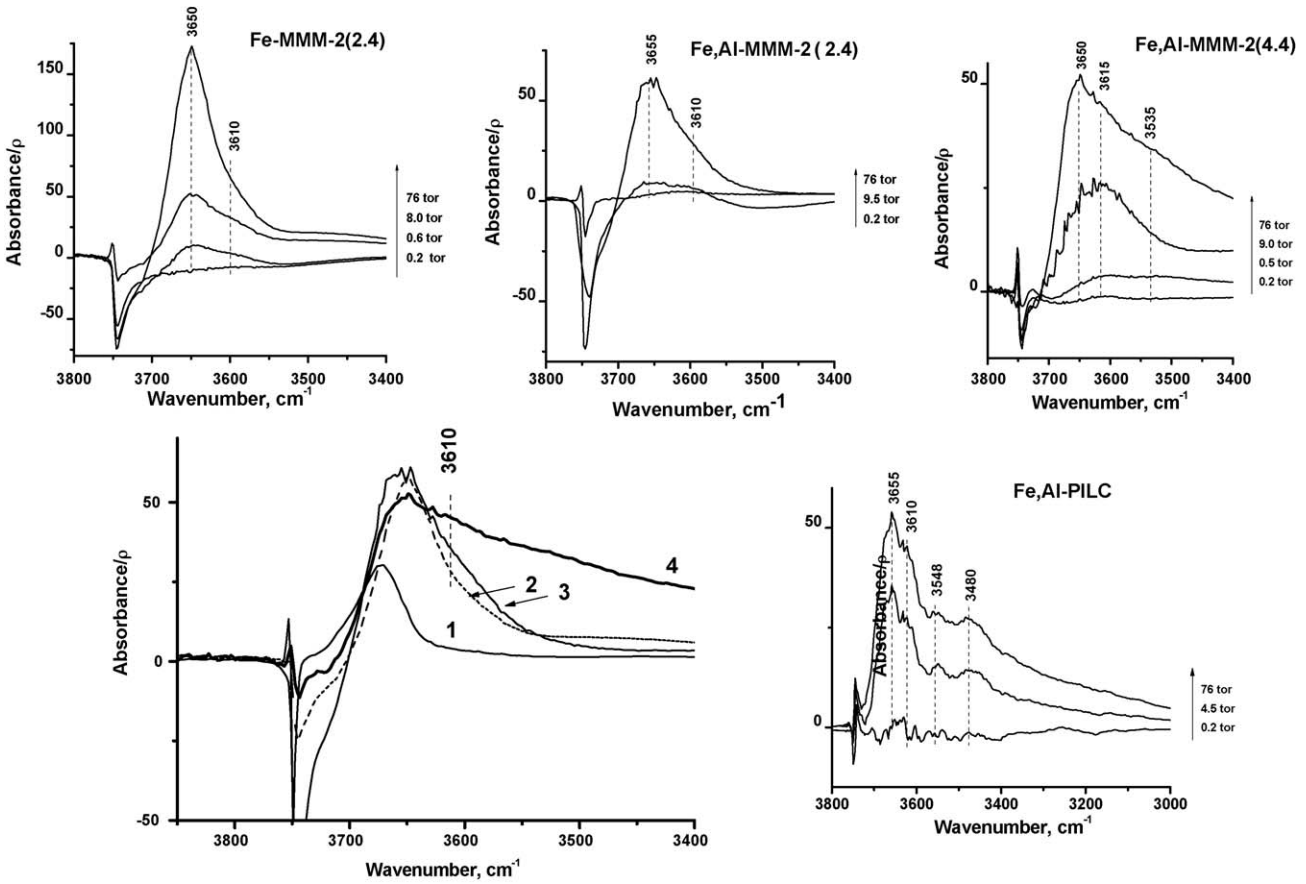

Fig. 5. FTIR difference spectra of adsorbed CO at nominally 80 K on the Fe-containing samples (O–H stretching region). The spectrum of Fe-containing samples before interaction with adsorbate molecules (Fig. 4) was used for background subtraction. Si-MMM-2 synthesized at pH 2.4 (1), Fe-MMM-2 synthesized at pH 2.4 (2), Fe,Al-MMM-2 synthesized at pH 2.4 (3) and Fe,Al-MMM-2 synthesized at pH 4.4 (4).

Huber [44] and Okuhara et al. [45] the band at 2265 cm^{-1} can be assigned to the weaker interaction between $CDCl_3$ and Si–OH group (complex A)

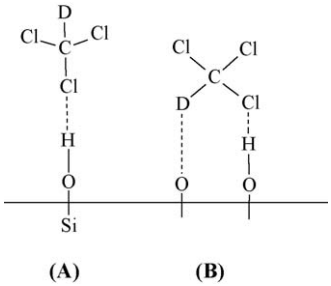

The bands in the region of 2240–2260 cm^{-1} can characterize basic sites with medium strength. Unfortunately, we have no any information about the state of these sites, but we can estimate their strength from the shift of ν_{C-D} using Eq. (1) [43]:

$$\log \Delta\nu_{C-D} = 0.0066 \cdot PA - 4.36 \quad (1)$$

The values of PA obtained from Eq. (1) allude to the fact that insertion of Al favours the increase in surface acidity Fe-containing samples. Fe,Al-MMM-2(4.4) possesses the stronger centres comparing to Fe-MMM-2(2.4). Note that the strength of surface sites is very similar for Fe,Al-MMM-2(4.4) and Fe,Al-PILC(4.4). Therefore it is reasonable to suppose that activity of Fe,Al-MMM-2(4.4) can be of the same order of magnitude with Fe,Al-PILC(4.4).

3.4. Catalytic activity of Fe-containing materials

The results of wet phenol oxidation with H_2O_2 over Fe-containing samples are presented in Table 4. Noteworthy, in

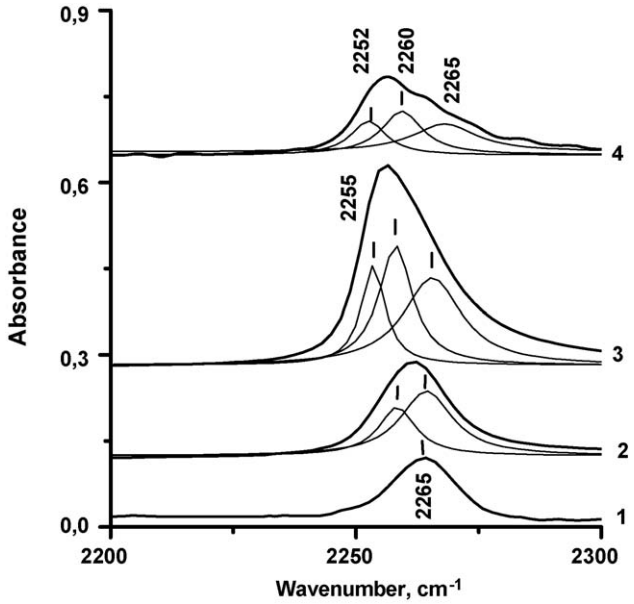

Fig. 6. FTIR difference spectra of adsorbed $CDCl_3$ on Si-MMM-2 synthesized at pH 2.4 (1), Fe-MMM-2 synthesized at pH 2.4 (2), Fe,Al-MMM-2 synthesized at pH 4.4 (3) and Fe,Al-PILC synthesized at pH 4.4 (4).

Table 3
Spectral characteristics (ν_{C-D}) of OH-groups for Fe-containing samples according to adsorption of $CDCl_3$.

	ν_{C-D} (cm^{-1})	$\Delta\nu_{C-D}$ (cm^{-1})	PA ($kJ\,mol^{-1}$)
$CDCl_3$	2268	–	–
Si-MMM-2	2265	3	733
Fe-MMM-2(2.4)	2265	3	733
	2260	8	797
Fe,Al-MMM-2(4.4)	2265	3	733
	2260	8	797
	2255	12	824
Fe,Al-PILC(4.4)	2265	3	733
	2260	8	797
	2252	16	843

operation we tried to establish the relationship between chemical composition, textural data and catalytic activity at pH 6.2. One can see from Table 4 that the catalytic activity of Fe,Al-MMM-2 is higher than that of Fe-MMM-2(2.4). The higher catalytic activity can be caused by the difference of H_2O_2 decomposition rates (Table 4). Interestingly, the increase in pH of synthesis of Fe,Al-MMM-2 can give a rise to the time of 50% H_2O_2 conversion that can be explained by the change in the iron state and type and strength of the surface acid sites. The mechanism of H_2O_2 decomposition can be described by the following scheme [46]:

$$\equiv Fe^{3+} + H_2O_2 \rightarrow \equiv Fe^{2+} + HO_2^{\bullet}/O_2^{-} + H^{+} \quad (2)$$

$$\equiv Fe^{2+} + H_2O_2 \rightarrow \equiv Fe^{3+} + HO^{\bullet} + OH^{-} \quad (3)$$

$$\equiv Fe^{3+} + HO_2^{\bullet}/O_2^{-} \rightarrow \equiv Fe^{2+} + O_2 + H^{+} \quad (4)$$

$$\equiv Fe^{3+} + HO^{\bullet} \rightarrow \equiv Fe^{2+} + OH^{-} \quad (5)$$

For homogeneous Fenton's systems it was demonstrated that reaction (3) is affected by reaction pH and type of ligands coordinated on Fe^{2+} [46,47]. Our experimental evidences allude to the fact that the increase of strength of basic sites of Fe-containing samples (PA) is accompanied with the increase of H_2O_2 degradation rate (Fig. 7).

Fig. 8 shows the kinetic curves of phenol and H_2O_2 consumption as well as the changes in pH of the phenol solution in the presence

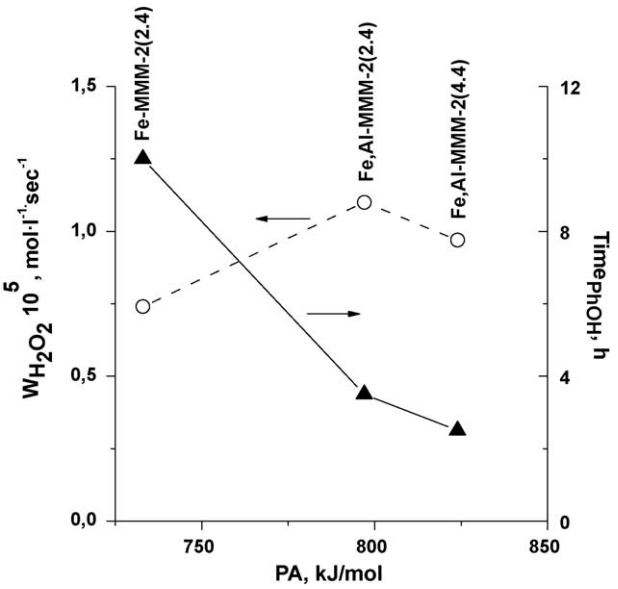

Fig. 7. Effect of strength of basic sites of Fe-containing samples (PA) on H_2O_2 decomposition rates and time of 100% conversion of PhOH.

of Fe-MMM-2(2.4) and Fe,Al-MMM-2(2.4). As can be seen from Fig. 8 the drop in pH occurs at the beginning of reaction. This pH decrease can be attributed to the formation of acid intermediate products. Consequently, the value of pH increases, most likely, due to the oxidation of these products. One can see that the catalytic activity of Fe,Al-MMM-2(2.4) was higher than that of Fe-MMM-2(2.4). This fact can be related to the difference in the strength of basic sites (Fig. 7). It can be also assumed that the difference of catalytic activities between Fe-MMM-2(2.4) and Fe,Al-MMM-2(2.4) can be caused by the effect of type and content of OH-groups (see Section 3.3). The insertion of Al leads to the increase in surface acidity and corresponding decrease of phenol adsorption (α_{PhOH}) on Fe,Al-MMM-2(2.4) (Table 4). Phenol, which is a weak acid (pK_a 10), adsorbs predominantly over weak Si–OH surface groups due to the binding forces prevailing between the phenol oxide and the positively charged surface of Fe-MMM-2(2.4). The effect of Al-content on α_{PhOH} was demonstrated for Al-bentonite [48,49] elsewhere.

Table 4
Phenol oxidation with H_2O_2 in the presence of Fe-containing samples.

Sample	PhOH oxidation[a]		Time[d] (min)	α_{phenol}[e] ($\times10^9$ mol m^{-2})	α_{ACDB}[f] ($\times10^9$ mol m^{-2})
	Time[b] (h)	Fe leaching[c] (wt.%)			
Without catalyst	>30	–	–	–	–
Fe-MMM-2(2.4)	10	0.2	180	215	4.2
Fe,Al-MMM-2(2.4)	3.5	6.7	120	66	2.2
Fe,Al-MMM-2(3.3)	3.5	5.2	128	62	2.5
Fe,Al-MMM-2(4.4)	2.5	<0.1	137	76	3.4
	1.0[g]	<0.1	–		
	2.5[h]	<0.1	–		
Fe,Al-PILC(4.4)	1.5[g]	<0.1	–	93	18.0
	0[h]	–	–		

[a] *Reaction conditions*: PhOH, 1 mM; H_2O_2, 14 mM; catalyst 1 g L^{-1}, pH 6.2, 60 °C.
[b] Time of 100% conversion of PhOH.
[c] The amount of iron leached from Fe-containing sample to solution (based on the initial iron content in the sample).
[d] Time of 50% conversion of 0.16 M H_2O_2 in the absence of phenol.
[e] Phenol adsorption on Fe-containing sample (50 mg) from aqueous solution (1 mM phenol, 10 ml) after 24 h at 25 °C.
[f] ACDB adsorption on Fe-containing sample (50 mg) from aqueous solution (0.1 mM ACDB, 5 ml) after 24 h at 25 °C.
[g] 50 °C.
[h] 40 °C.

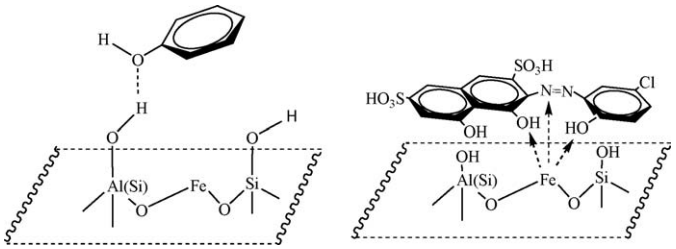

Notwithstanding the kinetic curve of PhOH oxidation with H_2O_2 over Fe-MMM-2(2.4) has induction period that is typical for all Fenton-like systems (Fig. 8). The insertion of Al leads to the disappearance of induction period that can be related with the increase in surface acidity of Fe,Al-MMM-2(2.4) which facilitates the sorption–desorption processes of reagents. Note that the content of Fe sites, accessible to reagents adsorption determined by ACDB adsorption [12] for Fe-MMM-2(2.4) is nearly twice as much as that for Fe,Al-MMM-2(2.4) (Table 4). The difference in adsorption values α_{PhOH} and α_{ACDB} relates with the difference of adsorption nature of PhOH and ACDB on Fe-containing materials. The ACDB adsorption can be depictured as coordination between OH- and N=N-groups of ACDB and Fe ion of on Fe-containing materials.

As one can see from Table 4, Fe,Al-MMM-2(4.4) is more stable with respect to the iron leaching compared to Fe-MMM-2(2.4), Fe,Al-MMM-2(2.4) and Fe,Al-MMM-2(3.3). There may be several reasons for the reduction of their stability. There are changes in the state of the active site on the catalyst surface, the difference of Al and Fe species localization (Section 3.2) and metal ion leaching induced by the reagents and/or products (Fig. 7).

According to Preethi et al. [15] Al content in Fe,Al-MCM-41 affected the selectivity of the products towards hydroquinone in phenol hydroxylation reaction (PhOH:H_2O_2 = 1:3 mol mol^{-1}). To examine this we studied the catalytic activity of the Fe,Al-MMM-2 for the hydroxylation of phenol. The phenol conversion and product selectivity are given in Table 5. The obtained results indicate conclusively that the more Al content in Fe,Al-MMM-2, the higher catalytic activity of Fe,Al-MMM-2 is observed. The Fe,Al-MMM-2(4.4) with Al/Fe = 12 was more active than Fe,Al-MMM-2(2.4) and Fe,Al-MMM-2(3.3) samples with Al/Fe = 6. The lower

Table 5
Phenol oxidation with H_2O_2 in the presence of Fe-containing samples[a].

	TON[b]	PhOH conversion (mol %)	Yield[c] (mol%)	
			CH	QH
Fe-MMM(2.4)	20	6	25	45
Fe,Al-MMM(2.4)	61	12	9	61
Fe,Al-MMM(3.3)	78	14	4	59
Fe,Al-MMM(4.4)	112	22	5	58

[a] *Reaction conditions*: PhOH, 0.1 M; H_2O_2, 0.2 M; catalyst 1 g L^{-1}, pH 6.2, 40 °C, 75 min.
[b] TON = moles of PhOH consumed/moles of Fe.
[c] Yield of CH and QH based on PhOH consumed.

selectivity to catechol over Fe,Al-MMM-2 is likely caused by impossibility of the side by side adsorption of phenol and hydrogen peroxide on the surface of Fe,Al-MMM-2 due to the change of the state and properties of surface sites. Moreover the increase of Al content in Fe,Al-MMM-2 favours strong adsorption of reagents on the surface due to the increase in the surface acidity, which can lead to polymerization of the hydrocarbons (Table 5). A similar effect of the Al content on catechol/hydroquinone ratio was also observed for Fe,Al-MCM-41 materials [15].

Of particular interest was a comparison of catalytic activity of mesoporous Fe,Al-MMM-2(4.4) with microporous Fe,Al-PILC(4.4) prepared from $FeAl_{12}^{7+}$ cation, which is the most active system in full phenol oxidation known in the literature. It was found that Fe,Al-MMM-2(4.4) was more active than Fe,Al-PILC(4.4) at 50 °C and especially at 40 °C, when Fe,Al-PILC(4.4) is not active (Table 4). These data point out not only the importance of surface acidity, but the textural data as well.

4. Conclusion

The Fe,Al-containing mesoporous mesophase silicate materials Fe,Al-MMM-2 have been synthesized under weak acidic conditions (pH 2.4–4.4) using Keggin type cation $[FeAl_{12}O_4(OH)_{24}(H_2O)_{12}]^{7+}$ ($FeAl_{12}^{7+}$) as Al and Fe sources. These materials were characterized by DR-UV–vis spectroscopy, XRD and N_2 adsorption. It was shown that textural properties of Fe,Al-MMM-2 can be controlled by pH of the synthetic mixture. Pore volume, surface area, and the mean

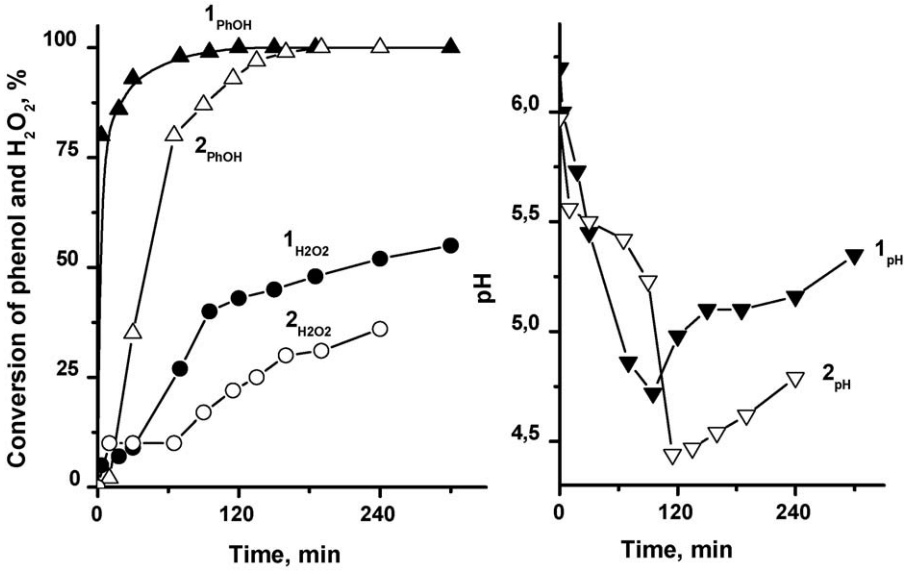

Fig. 8. The phenol and H_2O_2 consumption and changes in pH of solution in phenol oxidation in the presence of Fe,Al-MMM-2 synthesized at pH 2.4 (1) and Fe-MMM-2 synthesized at pH 2.4 (2) (catalyst 1.0 g L^{-1}, phenol 1 mM, H_2O_2 14 mM, pH 6.2, 70 °C).

pore diameter of Fe,Al-MMM-2(4.4) are lower than that of Fe,Al-MMM-2(2.4) and Fe,Al-MMM-2(3.3) due to the instability of $FeAl_{12}^{7+}$ cation at pH 2.3 and 3.3. The state of surface sites and their properties for Fe,Al-MMM-2 were analyzed by CO and $CDCl_3$ adsorbed as probe molecules in combination with IR spectroscopy. It was found that the state and properties of surface sites of Fe,Al-MMM-2 can be adjusted by pH of the synthetic mixture. The state of functional groups is similar for mesoporous Fe,Al-MMM-2(4.4) and microporous Fe,Al-pillared clay (Fe,Al-PILC(4.4)) due to the utilization of mixed $FeAl_{12}^{7+}$ cation for their synthesis.

Fe,Al-MMM-2 samples were tested in wet phenol oxidation with H_2O_2 (PhOH:H_2O_2 1:14 and 1:2 mol mol^{-1}) and H_2O_2 degradation. It was found that the increase in Al content favours the increase in catalytic activity in all reactions. It was demonstrated that the increase of the strength of basic sites of Fe-containing samples detected with $CDCl_3$ adsorption leads to the increasing of H_2O_2 degradation rate. Insertion of Al leads to the increase of surface acidity due to the changes of type and content of OH-groups which facilitate the sorption–desorption processes of reagents. Because of these changes the catalytic activity of Fe,Al-MMM-2(2.4) is higher than that of Fe-MMM-2(2.4). It was demonstrated that in the hydroxylation of phenol selectivity towards hydroquinone can be varied by increasing of Al content in sample. In full phenol oxidation with H_2O_2 Fe,Al-MMM-2(4.4) was found to be more active comparing to Fe,Al-PILC(4.4) in full phenol oxidation with H_2O_2.

Acknowledgement

Financial support of Russian Foundation for Basic Research under Grant 08-08-00729-a is acknowledged with gratitude. We thank Dr. A.V. Golovin for ^{27}Al NMR measurements.

References

[1] K. Fajerwerg, H. Debellefontaine, Appl. Catal. B.: Environ. 10 (1996) L229.
[2] G. Centi, S. Perathoner, T. Torre, M.G. Verduna, Catal. Today 55 (2000) 61.
[3] K. Pirkanniemi, M. Sillanpää, Chemosphere 48 (10) (2002) 1047.
[4] A. Corma, Chem. Rev. 97 (1997) 2373.
[5] Y. Wang, Q. Zhang, T. Shishido, K. Takehira, J. Catal. 209 (2002) 186.
[6] P. Ratnasamy, R. Kumar, Catal. Today 9 (1991) 329.
[7] T. Kawabata, Y. Ohishi, S. Itsiki, N. Fujisaki, T. Shishido, K. Takaki, Q. Zhang, Y. Wang, K. Takehira, J. Mol. Catal. A: Chem. 236 (2005) 99.
[8] F. Martinez, G. Calleja, J.A. Melero, R. Molina, Appl. Catal. B: Environ. 66 (2006) 198.
[9] R. Molina, F. Martinez, J.A. Melero, D.H. Bremner, A.G. Chakinala, Appl. Catal. B: Environ. 60 (2006) 181.
[10] L. Xianga, S. Royer, H. Zhang, J.-M. Tatibouet, J. Barrault, S. Valange, J. Hazard. Mater. 172 (2009) 1175.
[11] M.N. Timofeeva, M.S. Mel'gunov, O.A. Kholdeeva, M.E. Malyshev, A.N. Shmakov, V.B. Fenelonov, Appl. Catal. B: Environ. 75 (3–4) (2007) 290.
[12] M.N. Timofeeva, S.Ts. Khankhasaeva, Yu.A. Chesalov, S.V. Tsibulya, V.N. Panchenko, E.Ts. Dashinamzhilova, Appl. Catal. B: Environ. 88 (1–2) (2009) 127.
[13] A. Vinu, K.U. Nandhini, V. Murugesan, W. Bohlmann, V. Umamaheswari, A. Poppl, M. Hartmann, Appl. Catal. A: Gen. 265 (2004) 1.
[14] H. Lim, J. Lee, S. Jin, J. Kim, J. Yoon, T. Hyeon, Chem. Commun. (2006) 463.
[15] M.E.L. Preethi, S. Revathi, T. Sivakumar, D. Manikandan, D. Divakar, A.V. Rupa, M. Palanichami, Catal. Lett. 120 (2008) 56.
[16] D. Zhao, G. Wang, Y. Yang, X. Guo, Q. Wang, J. Ren, Clay Clay Miner. 41 (1993) 317.
[17] A. Oszko, J. Kiss, I. Kiricsi, Phys. Chem. Chem. Phys. 1 (1999) 2565.
[18] R.B. Martin, J. Inorg. Biochem. 44 (1991) 141.
[19] J.W. Akitt, N.N. Greenwood, B.L. Kladelwal, G.D. Lester, J. Chem. Soc., Dalton Trans. (1972) 604.
[20] A. Schutz, W.E.E. Stone, G. Pongelet, J.J. Fripiat, Clay Clay Miner. 35 (1987) 251.
[21] T.J. Pinnavaia, M.S. Tzou, S.D.L. Landau, R.H. Raythatha, J. Mol. Catal. 27 (1984) 195.
[22] Q.S. Huo, D.I. Margolese, G.D. Stucky, Chem. Mater. 8 (5) (1996) 1147.
[23] C.A. Fyfe, G. Fu, J. Am. Chem. Soc. 117 (1995) 9709.
[24] J.S. Beck, J.C. Vartuli, W.J. Roth, M.E. Leonowicz, C.T. Kresge, K.D. Schmitt, C.T.W. Chu, D.H. Olson, E.W. Shepard, S.B. McCullen, J.B. Higgins, J.L. Schlenker, J. Am. Chem. Soc. 114 (1992) 10834.
[25] M. Busio, J. Janchen, J.H.C. van Hoof, Micropor. Mater. 5 (1995) 211.
[26] D. Zhao, Y. Yang, X. Guo, Inorg. Chem. 31 (1992) 4727.
[27] J. Duan, J. Gregory, Adv. Colloid Interface Sci. 100–102 (2003) 475.
[28] A. Gil, M.A. Vicente, S.A. Korili, J. Catal. 229 (2005) 119.
[29] Q. Zhang, Y. Wang, S. Itsuki, T. Shishido, K. Takehira, Chem. Lett. 30 (2001) 946.
[30] Y. Li, Zh. Feng, Y. Lian, K. Sun, L. Zhang, G. Jia, Q. Yang, C. Li, Micropor. Mesopor. Mater. 84 (2005) 41.
[31] G. Spoto, A. Zecchina, G. Berlier, S. Bordiga, M.G. Clerici, L. Basini, J. Mol. Catal. A: Chem. 158 (2000) 107.
[32] E.J.M. Hensen, Q. Zhu, R.M. Hendrix, A.R. Overweg, P.J. Kooyman, M.V. Sychev, R.A. van Santen, J. Catal. 221 (2004) 560.
[33] M.S. Kumar, J. Perez-Ramırez, M.N. Debbagh, B. Smarsly, U. Bentrup, A. Bruckner, Appl. Catal. B: Environ. 62 (2006) 244.
[34] S.E. Dapurkar, S.K. Badamali, P. Selvam, Catal. Today 68 (2001) 63.
[35] S. Borgiga, R. Buzzoni, F. Geobaldo, C. Lamberti, E. Giamello, A. Zecchina, G. Leofanti, G. Petrini, G. Tozzola, G. Vlaic, J. Catal. 158 (1996) 486.
[36] K.I. Hadjiivanov, G.N. Vayssilov, Adv. Catal. 47 (2002) 307.
[37] P. Wu, T. Komatsu, T. Yashima, Micropor. Mater. 20 (1998) 139.
[38] C.T.W. Chu, C.D. Chang, J. Phys. Chem. 89 (1985) 1569.
[39] R. Kumar, A. Thangaraj, R.N. Bhat, P. Ratnasamy, Zeolites 10 (2) (1990) 85.
[40] J. Cejka, B. Wichterlova, Catal. Rev. 44 (3) (2002) 375.
[41] H. Knozinger, S. Huber, J. Chem. Soc., Faraday Trans. 94 (15) (1998) 2047.
[42] M. Sigl, S. Ernst, J. Weitkamp, H. Knozinger, Catal. Lett. 45 (1997) 27.
[43] E.A. Paukshtis, N.S. Kotsarenko, L.G. Karakchiev, React. Kinet. Catal. Lett. 12 (3) (1979) 315.
[44] H. Knozinger, S. Huber, J. Chem. Soc., Faraday Trans. 94 (1998) 2047.
[45] T. Okuhara, N. Mizuno, M. Misono, Adv. Catal. 41 (1996) 113.
[46] J.J. Pignatello, E. Oliveros, A. MacKay, Crit. Rev. Environ. Sci. Technol. 36 (2006) 1.
[47] J.C. Barreiro, M.D. Capelato, L. Martin-Neto, H.C.B. Hansen, Water Res. 41 (1) (2007) 55.
[48] M. Altunlu, S. Yapar, Colloids Surf. A: Physicochem. Eng. Aspects 306 (2007) 88.
[49] S. Al-Asheh, F. Banat, L. Abu-Aitah, Sep. Purif. Technol. 33 (2003) 1.